Dayside Pc2 waves associated with flux transfer events in a 3D hybrid-Vlasov simulation

F. Tesema[1], M. Palmroth[1,2], L. Turc[1], H. Zhou[1], G. Cozzani[1], M. Alho[1], Y. Pfau-Kempf[1], K. Horaites[1], I. Zaitsev[1], M. Grandin[1], M. Battarbee[1], U. Ganse[1], A. Workayehu[1], J. Suni[1], K. Papadakis[1], M. Dubart[1], V. Tarvus[1]

[1]Department of Physics, University of Helsinki, Helsinki, Finland
[2]Finnish Meteorological Institute, Space and Earth Observation Centre, Helsinki, Finland

Key Points:

- Dayside Pc2 waves (> 0.1 Hz) have been detected in a 3D hybrid-Vlasov simulation.
- These waves exhibit lower intensity within the magnetosphere at noon, compared to the prenoon and postnoon sectors.
- Pc2 waves observed in the simulation are associated with largest and fast moving flux transfer events initiated by subsolar reconnection.

Corresponding author: Fasil Tesema, `fasil.kebede@helsinki.fi`

Abstract

Flux transfer events (FTEs) are transient magnetic flux ropes at Earth's dayside magnetopause formed due to magnetic reconnection. As they move across the magnetopause surface, they can generate disturbances in the ultra-low frequency (ULF) range, which then propagate into the magnetosphere. This study provides evidence of ULF waves in the Pc2 wave frequency range caused by FTEs during dayside reconnection using a global 3D hybrid-Vlasov simulation (Vlasiator). These waves resulted from FTE formation and propagation at the magnetopause are particularly associated with large, rapidly moving FTEs. The wave power is stronger in the morning than afternoon, showing local time asymmetry. In the pre and postnoon equatorial regions, significant poloidal and toroidal components are present alongside the compressional component. The noon sector, with fewer FTEs, has lower wave power and limited magnetospheric propagation.

Plain Language Summary

The Earth's magnetosphere is a dynamic region shaped by the interplay between the solar wind and Earth's magnetic field. This interaction occurs at the boundary of the magnetosphere (magnetopause) through a process known as magnetic reconnection, giving rise to Flux Transfer Events (FTEs), which are magnetic structures that carry flux and energy into the magnetosphere. These FTEs form either in sudden bursts, patchy patterns or in a continuous, and relatively stable way making the magnetopause surface dynamic. As the FTEs move along the boundary of the magnetosphere, they create compressed regions and lead to wave generation that can extend into the magnetosphere. The study uses an advanced 3D hybrid-Vlasov simulation model to analyze waves originated from FTE formation and propagation at the magnetopause. We find that rapidly moving and large FTEs have a significant impact on the magnetopause, leading to the generation of ULF waves with frequency above 0.1 Hz. This shows first direct evidence supporting previous theoretical speculations regarding the ability of FTEs to generate waves near the magnetopause.

1 Introduction

Ultra low-frequency (ULF) waves in the Earth's magnetosphere play a crucial role in shaping the dynamics of radiation belts (Zong et al., 2017; Ripoll et al., 2020). The global occurrence and spatial distribution of these waves have captured considerable attention due to their role in transport and couple energy between solar wind and magnetosphere, energisation and loss of radiation belt particles (Menk et al., 2011). The literature extensively covers the generation mechanisms of ULF waves, which are primarily linked to fluctuations in the solar wind on the dayside, including pressure pulses and Kelvin-Helmholtz instability, as well as magnetospheric processes, such as substorms and other instabilities occurring on the nightside in the magnetotail (McPherron, 2005; Hwang & Sibeck, 2016; Bentley et al., 2018).

Numerous studies have proposed that the formation and propagation of flux transfer events (FTEs) along the surface of the magnetopause could compress the magnetic field and launch ULF waves in the Pc3 to Pc5 range (100–500 seconds) into the magnetosphere (Russell & Elphic, 1979; Glasmeier et al., 1984; Gillis et al., 1987; J. Liu et al., 2008; Bentley et al., 2018). This could arise due to the energy conversion related to magnetopause reconnection and the draping of magnetic field lines by FTEs along the magnetopause's surface (Arnoldy et al., 1988; Yagodkina & Vorobjev, 1997; Hwang, 2015). Furthermore, when the resulting quasi-periodic perturbations in the Pc3 to Pc5 range reach a sufficient magnitude, the FTE-generated compressional fast mode waves can propagate into the magnetosphere, and ultimately give rise to inner magnetospheric waves (Russell & Elphic, 1979; Gillis et al., 1987; Hwang & Sibeck, 2016).

Several studies have demonstrated that dayside reconnection can occur in either bursty and patchy patterns or in a continuous or quasi-steady manner with multiple reconnection points or separator lines occurring sequentially (e.g. Hasegawa et al., 2006, 2010; Fear et al., 2008; Tan et al., 2011; Hoilijoki et al., 2017; Walsh et al., 2017; H. Wang et al., 2019; Pfau-Kempf et al., 2020; Trattner et al., 2021). This deforms the magnetopause, creating recurring FTEs that are often accompanied by ULF pulsations at the magnetopause (Yagodkina & Vorobjev, 1997). Measurements from off-equatorial magnetospheric regions (Y. H. Liu et al., 2012) and research based on indirect observations (Kokubun et al., 1988; Arnoldy et al., 1988; Yagodkina & Vorobjev, 1997) have speculated that FTEs could also generate waves in the Pc1-2 frequency range. However, the direct link between waves in the frequency range above Pc3 and FTEs has not been made. This paper establishes the first direct link between Pc2 waves and the propagation and formation of FTEs on the dayside, utilizing a 3D hybrid-Vlasov simulation.

2 Model

In this study, we used the Vlasiator simulation (Palmroth et al., 2023), a global hybrid-Vlasov model described in Von Alfthan et al. (2014),Palmroth et al. (2018), and Ganse et al. (2023). Vlasiator self-consistently models the global ion dynamics using a 6D phase space (3D in physical space and 3D in velocity space) while electrons are treated as a charge-neutralizing fluid. The Ohm's law includes the convective, Hall, and electron pressure terms assuming an adiabatic electron fluid. Further implementation details of Vlasiator can be found in Palmroth et al. (2018).

The simulation was carried out in a domain defined by the boundaries $x = [-110.5, 50.2]R_E$, $y = [-57.8, 57.8]R_E$, $z = [-57.8, 57.8]R_E$, with R_E corresponding to the Earth's radius of 6371 km, encompassing the near-Earth solar wind, the dayside magnetopshere and an extended magnetotail and based on Geocentric Solar Ecliptic (GSE) coordinate system. The inner boundary was a near-ideal conducting sphere at a distance of 4.7 R_E, and the simulation employed adaptive mesh refinement (AMR) with three levels of spatial resolution, the highest resolution (0.16 R_E) around the magnetopause and magnetotail current sheet (Ganse et al., 2023). The simulation setup incorporated constant and homogeneous solar wind conditions, with the solar wind velocity of 750 kms^{-1} along the -x direction, a purely southward interplanetary magnetic field of 5 nT, a solar wind density of $n_{sw} = 1$ cm^{-3}, a solar wind temperature of $T_{sw} = 5 \times 10^5$ K, and an Alfvénic Mach number of $M = 6.9$.

Vlasiator's capability to resolve kinetic physics in detail results, among others, in its capability to reproduce the velocity distribution function in detail, as many of the kinetic physics and waves arise from the higher energy populations that are well resolved both in space and in velocity space (see Palmroth et al., 2023). Vlasiator has been shown to capture various ion kinetic phenomena (Hoilijoki et al., 2017; Pfau-Kempf et al., 2018, 2020). Additionally, several studies have validated their findings from Vlasiator using satellite observations (e.g. Palmroth et al., 2015; Pfau-Kempf et al., 2016; Akhavan-Tafti et al., 2020; Palmroth et al., 2021; Takahashi et al., 2021; Grandin et al., 2023).

3 Results

In this section, we present findings from the simulation described above, conducted for a duration of 1506 seconds. Our analysis considers data collected after the initialization phase, 662 seconds of the simulation. To characterize Pc2 waves in the simulation, we remove the background magnetic field by subtracting a moving average calculated over an interval much longer than the period of the ULF waves of interest. In this work we are interested in the frequency range above 0.1 Hz. Thus, the window for the moving average is set to 100 seconds, which can also capyure ULF waves with frequencies down to 0.006 Hz including those in the Pc4 range. We denote this magnetic field

variation vector, with the background subtracted, as $\delta\mathbf{B}$. All field parameters are transformed into local magnetic field-aligned coordinates (FAC) following the method outlined in Regi et al. (2017). The FAC system has three axes: one axis aligned with the local magnetic field direction (δB_p) and two axes perpendicular to it, along the radial (δB_r) and azimuthal directions (δB_a). In addition to the FAC system we also used the LMN coordinate system and the contouring method described in Alho et al. (2023) to identify FTE axes and their distributions. In this coordinate system L is along the maximum local variation of the magnetic field, N is orthogonal to L and approximately normal to the magnetopause current sheet, and M completes the right-handed orthonormal system. We also used the gradient of the normal magnetic field around the magnetopause as a proxy to determine the size of FTEs.

3.1 ULF waves near the magnetopause

To investigate the generation of Pc2 waves near passing FTEs, in Figure 1 we present a case study involving a virtual satellite situated at coordinates $[x = 8.95, y = -3.5, z = 1.57]R_E$ within the magnetosphere (indicated by a blue star). This virtual satellite observes magnetic field pulsations, and Figure 1 (b) and (c) depict the variations of the parallel magnetic field component (δB_p) and its wavelet power spectrum calculated using Morlet wavelet (Torrence & Compo, 1998). The wavelet power spectrum shows enhanced wave power in two distinct frequency bands: one localized in the frequency range between 0.1–0.3 Hz with a peak of 0.125 Hz (corresponding to Pc2 waves with an 8-second period), and another between 5–20 mHz with a peak at 10 mHz, corresponding to Pc4 waves. Our focus in this study is on the Pc2 waves. We also present a movie of these waves on three planes which are associated with prenoon, noon and postnoon periods (see Movie S1 in supplementary information). In the movie, Pc2 waves represented by δB_p are shown on planes at $y = 3.5R_E$ (postnoon), $y = 0R_E$ (noon), and $y = -3.5R_E$. The waves are originated from the magnetopause and propagating into the magnetosphere, and are more prominent in the post and prenoon planes.

In the Earth's magnetosphere, ULF waves typically exhibit a combination of polarizations, including compressional, toroidal, and poloidal modes (Lee & Lysak, 1989; McPherron, 2005). Figure 1 (d-f) displays the three polarization components (compressional, toroidal, and poloidal) after filtering using a 5th order band-pass Butterworth filter within the frequency range of [0.1−−0.5] Hz. The poloidal mode involves radial magnetic field pulsations and azimuthal electric field fluctuations, while the toroidal mode features variations in azimuthal magnetic field and radial electric field. The compressional mode is associated with oscillations mainly in the parallel magnetic field component and azimuthal electric field. Notably, there is significant interaction between compressional and poloidal oscillations, as both involve field line oscillations in the radial direction (Lee & Lysak, 1989). From all the three panels, starting around 870 seconds into the simulation, significant pulsation amplitudes occur periodically. The compressional component exhibits the highest amplitude, reaching up to $|\delta B_p| = 0.45$ nT, $|\delta E_a| = 0.44$ mV/m, while the poloidal and toroidal components have maximum amplitudes of $|\delta B_r| = 0.21$ nT, $|\delta E_r| = 0.38$ mV/m and $|\delta B_a| = 0.16$ nT, $|\delta E_a| = 0.44$ mV/m, respectively. Notably, the compressional and poloidal components feature three distinct wave packets during the time intervals of 870–1070, 1100–1200, 1200–1300, and 1300–1400 seconds.

To further investigate the spatial distribution of Pc2 waves depicted in Figure 1 (c), Figure 2 presents the distribution of wave power, averaged over the higher frequency band ([0.1–0.5] Hz) with a similar approach used in Turc, Zhou, et al. (2022). This distribution is shown across three distinct planes in the dayside magnetosphere, with data collected after 800 seconds into the simulation when Pc2 waves first become apparent in the magnetosphere. The three polarization components (δB_p, δB_a, and δB_r) were extracted from planes at $y = 3.5R_E$ (postnoon), $y = 0R_E$ (noon), and $y = -3.5R_E$ (prenoon). In the magnetosheath, the noon sector exhibits considerably higher compres-

sional and poloidal mean wave power than the other sectors. In contrast, within the magnetosphere, the prenoon sector shows the highest values for all polarization components, followed by the postnoon sector. Compressional wave modes dominate over toroidal and poloidal Pc2 ULF waves in the pre- and postnoon sectors, with the latter showing lower wave power, as demonstrated in Figure 2(b), (c), (h), and (i). The poloidal and toroidal modes were not detected deep within the magnetosphere near the magnetospheric equatorial plane. Additionally, the mean wave power significantly decreases as we go towards the cusp in both hemispheres. Despite the higher values of all components in the noon sector of the magnetosheath, the noon sector within the magnetosphere lacks significant wave power. Overall, the poloidal and toroidal components are restricted within the region between magnetopause and $x = 8R_E$, however, the compressional mode is seen beyond $x = 8R_E$ into the magnetosphere, especially in the prenoon sector ($Y = -3.5R_E$ plane).

3.2 Origin of Pc2 waves

To investigate the origin of the Pc2 waves depicted in Figure 2, in Figure 3 we demonstrate a correspondence between the FTEs along the magnetopause surface and the waves. We identified FTEs at a virtual spacecraft location approximately one Earth radius away in the x direction from where the waves are depicted in Figure 1(a) (blue star), near the magnetopause surface at coordinates $[x = 10.05, y = -3.5, z = 1.57]R_E$. FTEs are typically recognized by the presence of a bipolar variation in the magnetic field component that is locally perpendicular to the magnetopause (Russell & Elphic, 1979; Paschmann et al., 1982). However, additional indicators, such as an increase in magnetic field strength on the magnetosheath side of the FTE or a decrease on the magnetosphere side, elevated total pressure, and an increase in plasma bulk velocity in the z direction, have also been used to identify FTEs (Paschmann et al., 1982; Zhang et al., 2011; Teh et al., 2017; Sun et al., 2019).

In Figure 3(a-d), the combination of the FTE-related parameters, including the magnetic field magnitude, the radial and normal components of the magnetic field, plasma density and pressure, the z-component of plasma velocity, and the derivative of the local normal magnetic field along the L direction are used to indicate the presence of FTEs (marked with vertical dashed lines). The variations in magnetic field magnitude, the bipolarity of B_r and B_N, along with peak pressure and density, collectively suggest the existence of FTEs. In panel (e) of this figure, we present the gradient of B_N along the local magnetic field direction (L) to indirectly infer the size of the passing FTE. The significant variation and bipolarity of this gradient, after 900 seconds, around 1100 seconds, and before 1300 seconds, are observed near the wave packets shown in the last panel of the Figure 3, indicating the presence of large FTEs passing by.

Upon comparing Figure 3 (f) with the supplementary Movie S1, it becomes evident that FTEs, as they move along the magnetopause surface, give rise to the Pc2 waves. These waves are initiated during FTEs characterized by a significantly higher z-direction plasma bulk velocity (panel (d)) and are notably absent when the velocity drops below 100 km/s. This distinction is particularly pronounced before the 900-second mark and during the period between 1200 and 1300 seconds. In addition, a visual comparison of FTE occurrences, distribution of O points from (Alho et al., 2023) method, in the three planes presented in the supplementary Figure S1 reveals a significant difference between the $Y = -3.5R_E$ and $Y = 3.5R_E$ planes when compared to the noon-midnight plane. This occurrence pattern mirrors the Pc2 wave power illustrated in Figure 2. The majority of FTE formations are localized within the range of $Z = \pm 4R_E$ on the three planes (refer to the supplementary information video).

In Figure 4, we further illustrate the link between the FTE motion and the wave patterns presented on the plane $Y = -3.5R_E$ (see movie S1). Figure 4 (a) is a stacked

plot representing the z-component of plasma bulk velocity along the northern hemisphere of the magnetopause surface. In panel (b) of this Figure we present the Pc2 wave stack plot along a curve parallel to the magnetopause surface and inside the magnetosphere that includes the blue star shown in Figure 1 (a). In addition, contour lines of X and O points are superimposed as described in the Alho et al. (2023). Figure 4 (c) shows a similar panel from Figure 1 (d).

Examining Figure 4 (b) and (c), we note that the first two wave packets observed during the time periods 900–1060 and 1100–1200 in panel (c) are accompanied by reconnection events (X points) occurring around the sub-solar point (within $1R_E$), as well as one or more FTEs occurring away from this region, which is clearly visible in Supplementary animation 1. The subsequent wave packet observed after 1300 seconds originates from the reconnection region, as no O points are observed during this time period and around the sub-solar point. It is also worth highlighting that the time periods before 750 seconds and after 1400 seconds lack X points around the sub-solar point. To provide a schematic illustrating the scenario we propose to explain the observations throughout the entire simulation, we have included a schematic representation in Figure 4 (d). This illustration shows three source regions: one at the leading edge of the diverging FTEs, another at the reconnection region, and potentially the trailing edge of the two FTEs. During the entire simulation period (see Movie S1), the Pc2 waves observed originate from either of these three sources or a combination thereof.

4 Discussion

In this study, we have shown direct evidence of a previously speculated source of Pc2 waves which are associated with the formation and passage of FTEs along the magnetopause surface. Using a hybrid-Vlasov simulation, we demonstrated that these waves exhibit large wave power in the compressional, toroidal, and poloidal components with the compressional component being notably more dominant near the magnetospheric equator in close proximity to the magnetopause. Furthermore, we establish a strong connection between the presence of Pc2 waves and the occurrence of large, high-velocity FTEs initiated through a sub-solar reconnection.

In our simulation, despite the steady southward IMF, the reconnection process appears to be dynamic, as previously reported in 2D and 3D hybrid-Vlasov simulations by Hoilijoki et al. (2017) and Pfau-Kempf et al. (2020), as shown in Movie S1 of the supplementary information. Consequently, FTEs are continuously generated and propagate along the magnetopause. It is important to note that all the solar wind parameters remain constant throughout the simulation period, ruling out the possibility of attributing the Pc2 waves observed in our study to solar wind variations (Usanova et al., 2012). While Kelvin-Helmholtz instability (KHI) can also generate ULF waves, their efficiency and persistence are notably enhanced when the IMF orientation is northward (Hwang, 2015; Kavosi & Raeder, 2015), which is not the case in our simulation. KHI also exist during southward IMF, however, they are thought to drive Pc4-5 waves (C. P. Wang et al., 2017; Kronberg et al., 2021). In addition, the process of ULF waves originating from foreshock-generated sources and propagating across the magnetopause (Turc, Roberts, et al., 2022) is excluded due to the strictly southward orientation of the IMF, preventing the formation of the foreshock in front of the magnetopause nose. Thus, we conclude that the origin of the observed waves in the vicinity of the magnetopause in our simulation is attributed to magnetic reconnection and FTE propagation at the magnetopause surface. We have also clearly demonstrated this direct connection between FTEs and their propagation during active sub-solar reconnection.

Using spectral analysis of magnetic field component fluctuations, we have demonstrated that Pc2 waves display significant wave power within a region of $3\,R_E$ distance from the magnetopause (Figure 2). In addition, we have observed that the wave power

in the magnetosphere is highest in the prenoon sector in all three polarization components followed by the postnoon and noon sectors. Our simulation results indicate that Pc2 waves have similar spatial distributions and magnetic local time (MLT) as those observed in previous observational based studies (Grison et al., 2021). The MLT occurrence of waves (between 0.1 and 2 Hz) in the vicinity of the magnetopause reported by Grison et al. (2021) showed similar characteristics to what we observed in our simulation. Additionally, Anderson et al. (1992) conducted a statistical analysis, revealing a higher occurrence rate of dayside Pc1-2 pulsations in the outer magnetosphere ($L > 7$) compared to the inner magnetosphere ($L < 5$), coinciding with the same region where we observe Pc2 waves in our simulation. FTE associated magnetic pulsations in the in $6 - 8$ seconds period (Pc2 range) of magnitude $0.1-0.2$ nT is also reported by Yagodkina and Vorobjev (1997).

The majority of investigations into ULF waves within the frequency range discussed in this article (referred to as Pc2) have typically associated their driving mechanisms with variations in solar wind parameters or temperature anisotropy resulting from the interaction between hot ions moving from the nighttime to the daytime side and the cold ions in the plasmasphere (Usanova et al., 2012; Tetrick et al., 2017; Remya et al., 2018). However, this research also suggests that Pc2 waves may originate locally from the formation and propagation of Flux Transfer Events (FTEs). While this paper does not delve into the processes underlying the formation and the most suitable model for describing the FTEs observed in the simulation, Figure 4 and the accompanying video showcase numerous instances of multiple reconnection X-lines. These X-lines are particularly prevalent in the region where high wave power was detected (Figure 4). Whether these reconnection sites or the motion of FTEs serve as the dominant sources of the waves remains an unanswered question within the scope of this study, emphasizing the need for further investigations.

5 Summary

This study utilizes a hybrid-Vlasov simulation to investigate dayside Pc2 waves in the outer magnetosphere when a purely southward IMF and steady fast solar wind hits the Earth's magnetosphere. The study found Pc2 waves above 0.1 Hz frequency linked to the formation and passage of FTEs across the dayside magnetopause. We established a direct link between these waves and the presence of large, rapidly moving FTEs generated during sub-solar reconnection. Moreover, the study identified a significant asymmetry in MLT wave power, with the prenoon sector exhibiting a greater dominance of Pc2 waves compared to the noon and postnoon sectors. Substantial wave polarization components in the poloidal and toroidal ULF modes were also detected in the off-equatorial regions of the magnetosphere.

6 Open Research

The Vlasiator simulation code is freely available for download at `https://github.com/fmihpc/vlasiator`. To reproduce the data utilized in this study, refer to a configuration file at Pfau-Kempf et al. (2022). The output of the simulation is stored in a customized file format accessible at GitHub repository: `https://github.com/fmihpc/vlsv`. For post-processing of the simulation in this study a Python package, Analysator, available at `https://github.com/fmihpc/analysator` (Battarbee et al., 2021) is used.

Acknowledgments
Vlasiator is developed by funding from the European Research Council Starting Grant 200141-QuESpace and Consolidator Grant 682068—PRESTISSIMO. We also appreciate the support provided by the CSC-IT Center for Science in Finland and the Partner-

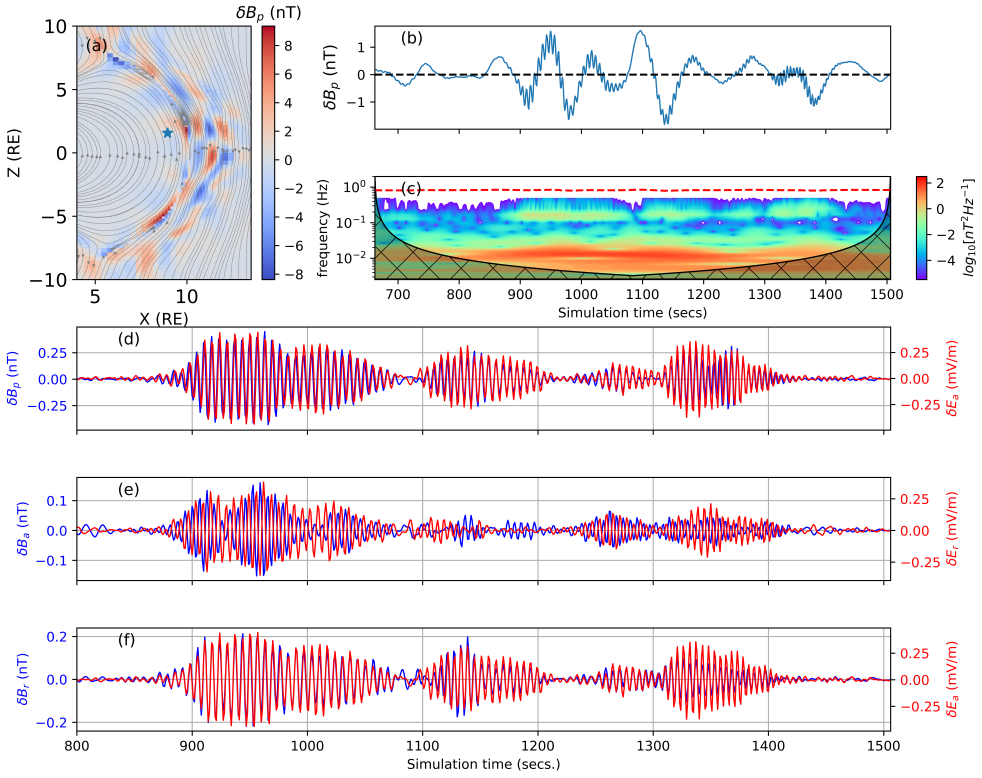

Figure 1. (a) variation of B in the parallel direction on $Y = -3.5R_E$ plane at $t = 956s$. (b) its time evolution from a virtual spacecraft located at $[x = 8.95, y = -3.5, z = 1.57]R_E$ the blue asterisk in (a), (c) Morlet wavelet transform of (b), shaded area is the cone of influence and the dashed red line is the local gyrofrequency. The lower three panels (d, e, and f) consist of polarization components (compressional, toroidal, and poloidal, respectively) of the magnetic field filtered in the Pc2 wave, $[0.1, 0.5]$ Hz, frequency range.

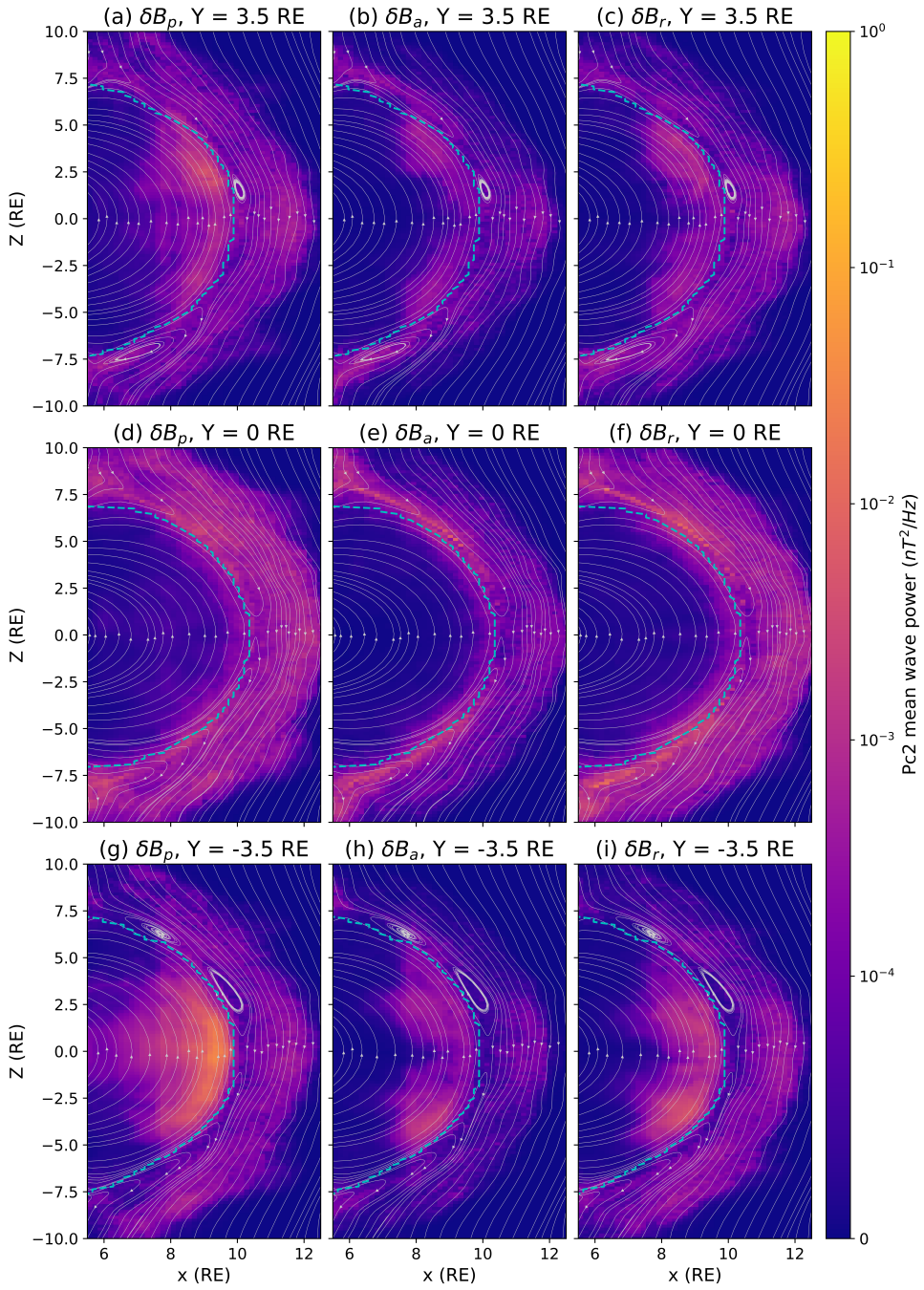

Figure 2. Spatial distribution of mean wave power in Pc2 range of compressional, toroidal, and poloidal components at the cross-sectional plane in the postnoon (top row), noon (mid row) and prenoon (bottom row) sectors, using the parallel, azimuthal, and radial component of the magnetic field. The cyan curve shows the approximate location of the magnetopause ($\beta^* = 1.2$) according to Brenner et al. (2021). The light gray magnetic field lines represent the magnetosphere condition at t = 1112 seconds into the simulation.

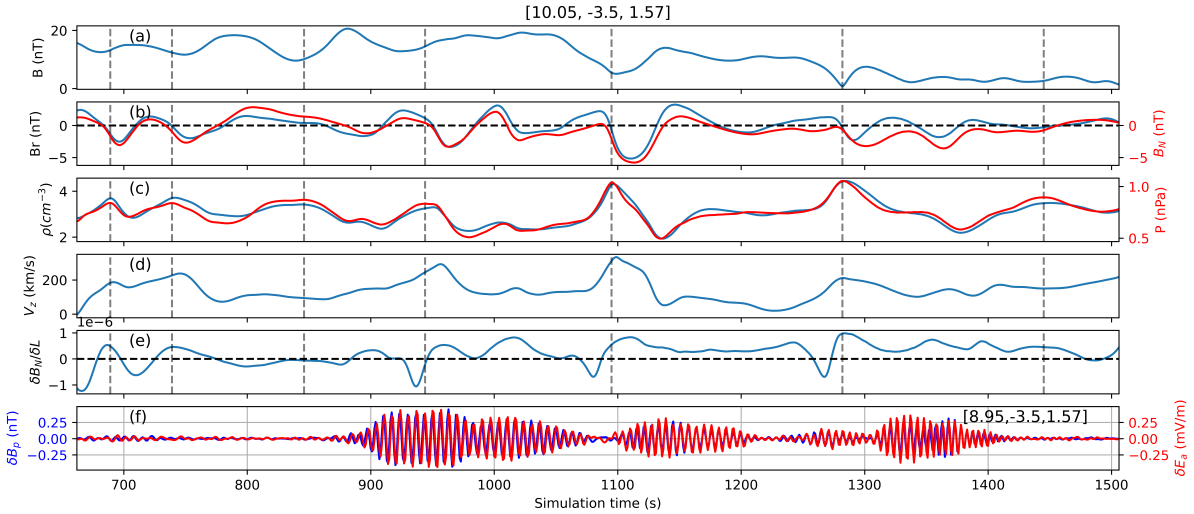

Figure 3. (a) Magnitude of magnetic field at the virtual spacecraft in the vicinity of the magnetopause at $[x = 10.05, y = -3.5, z = 1.57]R_E$, (b) radial and local normal N component of magnetic field, (c) proton density and pressure, (d) the z-component of proton velocity, and (e) the gradient of the local normal magnetic field in the local magnetic field direction. The vertical dashed lines show the time of FTEs at the virtual spacecraft location based on pressure peaks. The last panel shows the compressional ULF pulsation in the Pc2 frequency range from a virtual spacecraft at the same location as Figure 1 (a).

ship for Advanced Computing in Europe (PRACE) Tier-0 supercomputer infrastructure in HLRS Stuttgart (project number PRACE-2019204998). Additional support came from Academy of Finland Grants 339327, 335554, 347795, 345701, and 336805. The contributions of M. Grandin (AERGELC'H project, Grant 338629), Y. Pfau-Kempf (KIMCHI project, Grant 339756), L. Turc (UNTWINE project, Grant 322544), V. Tarvus (UNTWINE project, Grant 353197), and H. Zhou (RESSAC project, 3-year research Grant 2020–2022) were supported by the Academy of Finland and the University of Helsinki. Wavelet software was provided by Grinsted et al. (2004), which is available at `http://noc.ac.uk/using-science/crosswavelet-wavelet-coherence`.

References

Akhavan-Tafti, M., Palmroth, M., Slavin, J. A., Battarbee, M., Ganse, U., Grandin, M., ... Stawarz, J. E. (2020, 7). Comparative Analysis of the Vlasiator Simulations and MMS Observations of Multiple X-Line Reconnection and Flux Transfer Events. *Journal of Geophysical Research: Space Physics*, *125*(7), e2019JA027410. doi: 10.1029/2019JA027410

Alho, M., Cozzani, G., Zaitsev, I., Kebede, F. T., Ganse, U., Battarbee, M., ... Palmroth, M. (2023). Finding reconnection lines and flux rope axes via local coordinates in global ion-kinetic magnetospheric simulations. *EGUsphere*, *2023*, 1–24. doi: 10.5194/egusphere-2023-2300

Anderson, B. J., Erlandson, R. E., & Zanetti, L. J. (1992, 3). A statistical study of Pc 1-2 magnetic pulsations in the equatorial magnetosphere: 1. Equatorial occurrence distributions. *Journal of Geophysical Research: Space Physics*, *97*(A3), 3075–3088. doi: 10.1029/91JA02706

Arnoldy, R. L., Engebretson, M. J., & Cahill, L. J. (1988, 2). Bursts of Pc 1-2 near the ionospheric footprint of the cusp and their relationship to flux transfer

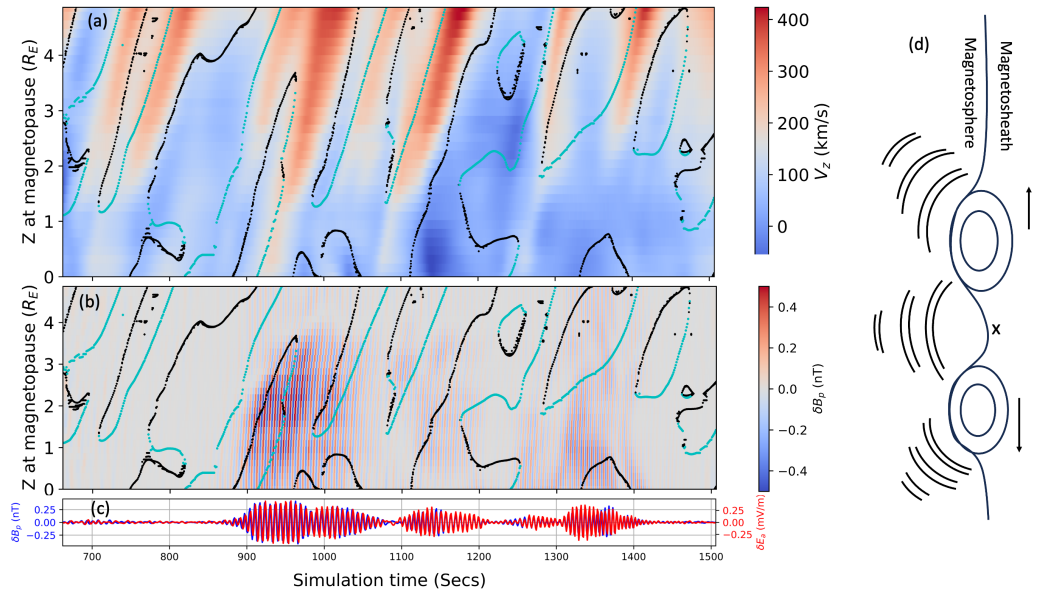

Figure 4. (a) A stacked plot showcasing the plasma bulk velocity from a curve along the Z-direction along the magnetopause surface, ranging from $Z = 0\,R_E$ to $Z = 5\,R_E$ on the plane $Y = -3.5\,R_E$, (b) a similar stacked plot but for the Pc2 wave resulting from pulsations in the parallel component of the magnetic field, occurring on a surface parallel to the magnetopause and situated inside the magnetosphere including the blue star at $Z = 1.57\,R_E$shown in Figure 1 (a), and (c) a replication of the panel as displayed in Figure 3 (f), (d) a cartoon illustrating different sources of waves discussed, as depicted in the accompanying video (Movie S1), X denotes the reconnection point. The contour lines in (a) and (b) are the X points (black) and O points (cyan).

events. *Journal of Geophysical Research: Space Physics*, *93*(A2), 1007–1016. doi: 10.1029/JA093IA02P01007

Battarbee, M., Hannuksela, O. A., Pfau-Kempf, Y., Alfthan, S. v., Ganse, U., Jarvinen, R., ... Grandin, M. (2021, 1). fmihpc/analysator: v0.9. doi: 10.5281/ZENODO.4462515

Bentley, S. N., Watt, C. E., Owens, M. J., & Rae, I. J. (2018, 4). ULF Wave Activity in the Magnetosphere: Resolving Solar Wind Interdependencies to Identify Driving Mechanisms. *Journal of Geophysical Research: Space Physics*, *123*(4), 2745–2771. doi: 10.1002/2017JA024740

Brenner, A., Pulkkinen, T. I., Al Shidi, Q., & Toth, G. (2021, 10). Stormtime Energetics: Energy Transport Across the Magnetopause in a Global MHD Simulation. *Frontiers in Astronomy and Space Sciences*, *8*, 180. doi: 10.3389/FSPAS.2021.756732/BIBTEX

Fear, R. C., Milan, S. E., Fazakerley, A. N., Lucek, E. A., Cowley, S. W., & Dandouras, I. (2008, 8). The azimuthal extent of three flux transfer events. *Annales Geophysicae*, *26*(8), 2353–2369. Retrieved from `www.ann-geophys.net/26/2353/2008/` doi: 10.5194/ANGEO-26-2353-2008

Ganse, U., Koskela, T., Battarbee, M., Pfau-Kempf, Y., Papadakis, K., Alho, M., ... Palmroth, M. (2023, 4). Enabling technology for global 3D + 3V hybrid-Vlasov simulations of near-Earth space. *Physics of Plasmas*, *30*(4), 42902. Retrieved from `https://pubs.aip.org/aip/pop/article/30/4/042902/2878614/Enabling-technology-for-global-3D-3V-hybrid-Vlasov` doi: 10.1063/5.0134387/2878614

Gillis, E. J., Rijnbeek, R., Kling, R., Speiser, T. W., & Fritz, T. A. (1987, 6). Do flux transfer events cause long-period micropulsations in the dayside magnetosphere? *Journal of Geophysical Research*, *92*(A6), 5820. doi: 10.1029/JA092iA06p05820

Glasmeier, K., Lester, M., Mier-Jedrzejowicz, W., Green, C., Rostoker, G., Orr, D., ... Amata, E. (1984, 8). Pc5 pulsations and their possible source mechanisms: a case study. *Journal of Geophysics*, *55*(1), 108–119. Retrieved from `https://journal.geophysicsjournal.com/JofG/article/view/205`

Grandin, M., Luttikhuis, T., Battarbee, M., Cozzani, G., Zhou, H., Turc, L., ... Palmroth, M. (2023). First 3D hybrid-Vlasov global simulation of auroral proton precipitation and comparison with satellite observations. *Journal of Space Weather and Space Climate*, *13*, 20. doi: 10.1051/SWSC/2023017

Grinsted, A., Moore, J. C., & Jevrejeva, S. (2004, 11). Application of the cross wavelet transform and wavelet coherence to geophysical time series. *Nonlinear Processes in Geophysics*, *11*(5/6), 561–566. doi: 10.5194/NPG-11-561-2004

Grison, B., Santolík, O., Lukačevič, J., & Usanova, M. E. (2021, 2). Occurrence of EMIC Waves in the Magnetosphere According to Their Distance to the Magnetopause. *Geophysical Research Letters*, *48*(3). doi: 10.1029/2020GL090921

Hasegawa, H., Sonnerup, B. U., Owen, C. J., Klecker, B., Paschmann, G., Balogh, A., & Rème, H. (2006, 3). The structure of flux transfer events recovered from Cluster data. *Annales Geophysicae*, *24*(2), 603–618. doi: 10.5194/ANGEO-24-603-2006

Hasegawa, H., Wang, J., Dunlop, M. W., Pu, Z. Y., Zhang, Q. H., Lavraud, B., ... Bogdanova, Y. V. (2010, 8). Evidence for a flux transfer event generated by multiple X-line reconnection at the magnetopause. *Geophysical Research Letters*, *37*(16). doi: 10.1029/2010GL044219

Hoilijoki, S., Ganse, U., Pfau-Kempf, Y., Cassak, P. A., Walsh, B. M., Hietala, H., ... Palmroth, M. (2017, 3). Reconnection rates and X line motion at the magnetopause: Global 2D-3V hybrid-Vlasov simulation results. *Journal of Geophysical Research: Space Physics*, *122*(3), 2877–2888. doi: 10.1002/2016JA023709

Hwang, K. J. (2015). Magnetopause Waves Controlling the Dynamics of Earth's Magnetosphere. *Journal of Astronomy and Space Sciences*, *32*(1), 1–11. doi: 10.5140/JASS.2015.32.1.1

Hwang, K. J., & Sibeck, D. G. (2016, 2). Role of Low-Frequency Boundary Waves in the Dynamics of the Dayside Magnetopause and the Inner Magnetosphere. *Low-Frequency Waves in Space Plasmas*, 213–239. doi: 10.1002/9781119055006.CH13

Kavosi, S., & Raeder, J. (2015, 5). Ubiquity of Kelvin–Helmholtz waves at Earth's magnetopause. *Nature Communications 2015 6:1*, *6*(1), 1–6. doi: 10.1038/ncomms8019

Kokubun, S., Yamamoto, T., Hayashi, K., Oguti, T., & Egeland, A. (1988). Impulsive Pi Bursts Associated with Poleward Moving Auroras Near the Polar Cusp. *Journal of geomagnetism and geoelectricity*, *40*(5), 537–551. doi: 10.5636/JGG.40.537

Kronberg, E. A., Gorman, J., Nykyri, K., Smirnov, A. G., Gjerloev, J. W., Grigorenko, E. E., ... Friel, M. (2021, 12). Kelvin-Helmholtz Instability Associated With Reconnection and Ultra Low Frequency Waves at the Ground: A Case Study. *Frontiers in Physics*, *9*, 738988. doi: 10.3389/FPHY.2021.738988/BIBTEX

Lee, D.-H., & Lysak, R. L. (1989, 12). Magnetospheric ULF wave coupling in the dipole model: The impulsive excitation. *Journal of Geophysical Research*, *94*(A12), 17097. doi: 10.1029/JA094iA12p17097

Liu, J., Angelopoulos, V., Sibeck, D., Phan, T., Pu, Z. Y., McFadden, J., ... Auster, H. U. (2008, 9). THEMIS observations of the dayside traveling compression region and flows surrounding flux transfer events. *Geophysical Research Letters*, *35*(17). doi: 10.1029/2008GL033673

Liu, Y. H., Fraser, B. J., & Menk, F. M. (2012, 9). Pc2 EMIC waves generated high off the equator in the dayside outer magnetosphere. *Geophysical Research Letters*, *39*(17). doi: 10.1029/2012GL053082

McPherron, R. L. (2005, 9). Magnetic pulsations: Their sources and relation to solar wind and geomagnetic activity. *Surveys in Geophysics*, *26*(5), 545–592. doi: 10.1007/S10712-005-1758-7/METRICS

Menk, F. W., Menk, & W., F. (2011). Magnetospheric ULF Waves: A Review. *dyma*, *3*, 223–256. doi: 10.1007/978-94-007-0501-2{_}13

Palmroth, M., Archer, M., Vainio, R., Hietala, H., Pfau-Kempf, Y., Hoilijoki, S., ... Eastwood, J. P. (2015, 10). ULF foreshock under radial IMF: THEMIS observations and global kinetic simulation Vlasiator results compared. *Journal of Geophysical Research: Space Physics*, *120*(10), 8782–8798. doi: 10.1002/2015JA021526

Palmroth, M., Ganse, U., Yann Pfau-Kempf, , Battarbee, M., Turc, L., Brito, T., ... Sebastian Von Alfthan, (2018, 8). Vlasov methods in space physics and astrophysics. *Living Reviews in Computational Astrophysics 2018 4:1*, *4*(1), 1–54. doi: 10.1007/S41115-018-0003-2

Palmroth, M., Pulkkinen, T. I., Ganse, U., Pfau-Kempf, Y., Koskela, T., Zaitsev, I., ... Nakamura, R. (2023, 6). Magnetotail plasma eruptions driven by magnetic reconnection and kinetic instabilities. *Nature Geoscience 2023 16:7*, *16*(7), 570–576. doi: 10.1038/s41561-023-01206-2

Palmroth, M., Raptis, S., Suni, J., Karlsson, T., Turc, L., Johlander, A., ... Osmane, A. (2021, 3). Magnetosheath jet evolution as a function of lifetime: Global hybrid-Vlasov simulations compared to MMS observations. *Annales Geophysicae*, *39*(2), 289–308. doi: 10.5194/ANGEO-39-289-2021

Paschmann, G., Haerendel, G., Papamastorakis, I., Sckopke, N., Bame, S. J., Gosling, J. T., & Russell, C. T. (1982). Plasma and magnetic field characteristics of magnetic flux transfer events. *Journal of Geophysical Research*, *87*(A4), 2159. doi: 10.1029/JA087IA04P02159

Pfau-Kempf, Y., Alfthan, S. v., Ganse, U., Sandroos, A., Battarbee, M., Koskela, T., ... Alho, M. (2022, 6). fmihpc/vlasiator: Vlasiator 5.2.1. Retrieved from https://zenodo.org/record/6782211 doi: 10.5281/ZENODO.6782211

Pfau-Kempf, Y., Battarbee, M., Ganse, U., Hoilijoki, S., Turc, L., von Alfthan, S., ... Palmroth, M. (2018, 5). On the importance of spatial and velocity resolution in the hybrid-Vlasov modeling of collisionless shocks. *Frontiers in Physics*, *6*(MAY), 44. doi: 10.3389/FPHY.2018.00044/BIBTEX

Pfau-Kempf, Y., Hietala, H., Milan, S. E., Juusola, L., Hoilijoki, S., Ganse, U., ... Palmroth, M. (2016). Evidence for transient, local ion foreshocks caused by dayside magnetopause reconnection. , *34*, 943–959. doi: 10.5194/angeo-34-943-2016

Pfau-Kempf, Y., Palmroth, M., Johlander, A., Turc, L., Alho, M., Battarbee, M., ... Ganse, U. (2020, 9). Hybrid-Vlasov modeling of three-dimensional dayside magnetopause reconnection. *Physics of Plasmas*, *27*(9), 092903. doi: 10.1063/5.0020685/5.0020685.MM.ORIGINAL.V1.MP4

Regi, M., Del Corpo, A., & De Lauretis, M. (2017, 1). The use of the empirical mode decomposition for the identification of mean field aligned reference frames. *Annals of Geophysics*, *59*(6), G0651. Retrieved from https://www.annalsofgeophysics.eu/index.php/annals/article/view/7067 doi: 10.4401/ag-7067

Remya, B., Sibeck, D. G., Halford, A. J., Murphy, K. R., Reeves, G. D., Singer, H. J., ... Thaller, S. A. (2018, 6). Ion Injection Triggered EMIC Waves in the Earth's Magnetosphere. *Journal of Geophysical Research: Space Physics*, *123*(6), 4921–4938. doi: 10.1029/2018JA025354

Ripoll, J., Claudepierre, S. G., Ukhorskiy, A. Y., Colpitts, C., Li, X., Fennell, J. F., & Crabtree, C. (2020, 5). Particle Dynamics in the Earth's Radiation Belts: Review of Current Research and Open Questions. *Journal of Geophysical Research: Space Physics*, *125*(5). Retrieved from https://onlinelibrary.wiley.com/doi/abs/10.1029/2019JA026735 doi: 10.1029/2019JA026735

Russell, C. T., & Elphic, R. C. (1979). ISEE observations of flux transfer events at the dayside magnetopause. *Geophysical Research Letters*, *6*(1), 33–36. doi: 10.1029/GL006I001P00033

Sun, T. R., Tang, B. B., Wang, C., Guo, X. C., & Wang, Y. (2019, 4). Large-Scale Characteristics of Flux Transfer Events on the Dayside Magnetopause. *Journal of Geophysical Research: Space Physics*, *124*(4), 2425–2434. doi: 10.1029/2018JA026395

Takahashi, K., Turc, L., Kilpua, E., Takahashi, N., Dimmock, A., Kajdic, P., ... Battarbee, M. (2021, 2). Propagation of Ultralow-Frequency Waves from the Ion Foreshock into the Magnetosphere During the Passage of a Magnetic Cloud. *Journal of Geophysical Research: Space Physics*, *126*(2), e2020JA028474. doi: 10.1029/2020JA028474

Tan, B., Lin, Y., Perez, J. D., & Wang, X. Y. (2011). Global-scale hybrid simulation of dayside magnetic reconnection under southward IMF: Structure and evolution of reconnection. *J. Geophys. Res*, *116*, 2206. doi: 10.1029/2010JA015580

Teh, W. L., Nakamura, T. K., Nakamura, R., Baumjohann, W., Russell, C. T., Pollock, C., ... Giles, B. L. (2017, 2). Evolution of a typical ion-scale magnetic flux rope caused by thermal pressure enhancement. *Journal of Geophysical Research: Space Physics*, *122*(2), 2040–2050. doi: 10.1002/2016JA023777

Tetrick, S. S., Engebretson, M. J., Posch, J. L., Olson, C. N., Smith, C. W., Denton, R. E., ... Fennell, J. F. (2017, 4). Location of intense electromagnetic ion cyclotron (EMIC) wave events relative to the plasmapause: Van Allen Probes observations. *Journal of Geophysical Research: Space Physics*, *122*(4), 4064–4088. doi: 10.1002/2016JA023392

Torrence, C., & Compo, P. (1998). A practical guide to wavelet analysis. *Bulletin of the American Meteorological Society*, 61–78. doi: 10.1175/1520-0477(1998)079

Trattner, K. J., Petrinec, S. M., & Fuselier, S. A. (2021, 3). The Location of Magnetic Reconnection at Earth's Magnetopause. *Space Science Reviews 2021 217:3*, *217*(3), 1–47. doi: 10.1007/S11214-021-00817-8

Turc, L., Roberts, O. W., Verscharen, D., Dimmock, A. P., Kajdič, P., Palmroth, M., ... Ganse, U. (2022, 12). Transmission of foreshock waves through Earth's bow shock. *Nature Physics 2022 19:1*, *19*(1), 78–86. doi: 10.1038/s41567-022-01837-z

Turc, L., Zhou, H., Tarvus, V., Ala-Lahti, M., Battarbee, M., Pfau-Kempf, Y., ... Palmroth, M. (2022, 9). A global view of Pc3 wave activity in near-Earth space: Results from hybrid-Vlasov simulations. *Frontiers in Astronomy and Space Sciences*, *9*, 989369. doi: 10.3389/FSPAS.2022.989369/BIBTEX

Usanova, M. E., Mann, I. R., Bortnik, J., Shao, L., & Angelopoulos, V. (2012, 10). THEMIS observations of electromagnetic ion cyclotron wave occurrence: Dependence on AE, SYMH, and solar wind dynamic pressure. *Journal of Geophysical Research: Space Physics*, *117*(A10), 10218. doi: 10.1029/2012JA018049

Von Alfthan, S., Pokhotelov, D., Kempf, Y., Hoilijoki, S., Honkonen, I., Sandroos, A., & Palmroth, M. (2014, 12). Vlasiator: First global hybrid-Vlasov simulations of Earth's foreshock and magnetosheath. *Journal of Atmospheric and Solar-Terrestrial Physics*, *120*, 24–35. doi: 10.1016/J.JASTP.2014.08.012

Walsh, B. M., Komar, C. M., & Pfau-Kempf, Y. (2017, 4). Spacecraft measurements constraining the spatial extent of a magnetopause reconnection X line. *Geophysical Research Letters*, *44*(7), 3038–3046. doi: 10.1002/2017GL073379

Wang, C. P., Thorne, R., Liu, T. Z., Hartinger, M. D., Nagai, T., Angelopoulos, V., ... Spence, H. E. (2017, 5). A multispacecraft event study of Pc5 ultralow-frequency waves in the magnetosphere and their external drivers. *Journal of Geophysical Research: Space Physics*, *122*(5), 5132–5147. doi: 10.1002/2016JA023610

Wang, H., Lin, Y., Wang, X., & Guo, Z. (2019, 7). Generation of kinetic Alfvén waves in dayside magnetopause reconnection: A 3-D global-scale hybrid simulation. *Physics of Plasmas*, *26*(7), 072102. doi: 10.1063/1.5092561

Yagodkina, O. I., & Vorobjev, V. G. (1997). Daytime high-latitude pulsations associated with solar wind dynamic pressure impulses and flux transfer events. *Journal of Geophysical Research: Space Physics*, *102*(A1), 57–67. doi: 10.1029/96JA01273

Zhang, H., Kivelson, M. G., Angelopoulos, V., Khurana, K. K., Walker, R. J., Jia, Y. D., ... Auster, H. U. (2011, 8). Flow vortices associated with flux transfer events moving along the magnetopause: Observations and an MHD simulation. *Journal of Geophysical Research: Space Physics*, *116*(A8), 8202. Retrieved from `https://agupubs.onlinelibrary.wiley.com/doi/10.1029/2011JA016500` doi: 10.1029/2011JA016500

Zong, Q., Rankin, ., & Zhou, . (2017, 11). The interaction of ultra-low-frequency pc3-5 waves with charged particles in Earth's magnetosphere. *Reviews of Modern Plasma Physics 2017 1:1*, *1*(1), 1–90. doi: 10.1007/S41614-017-0011-4

Figure1.

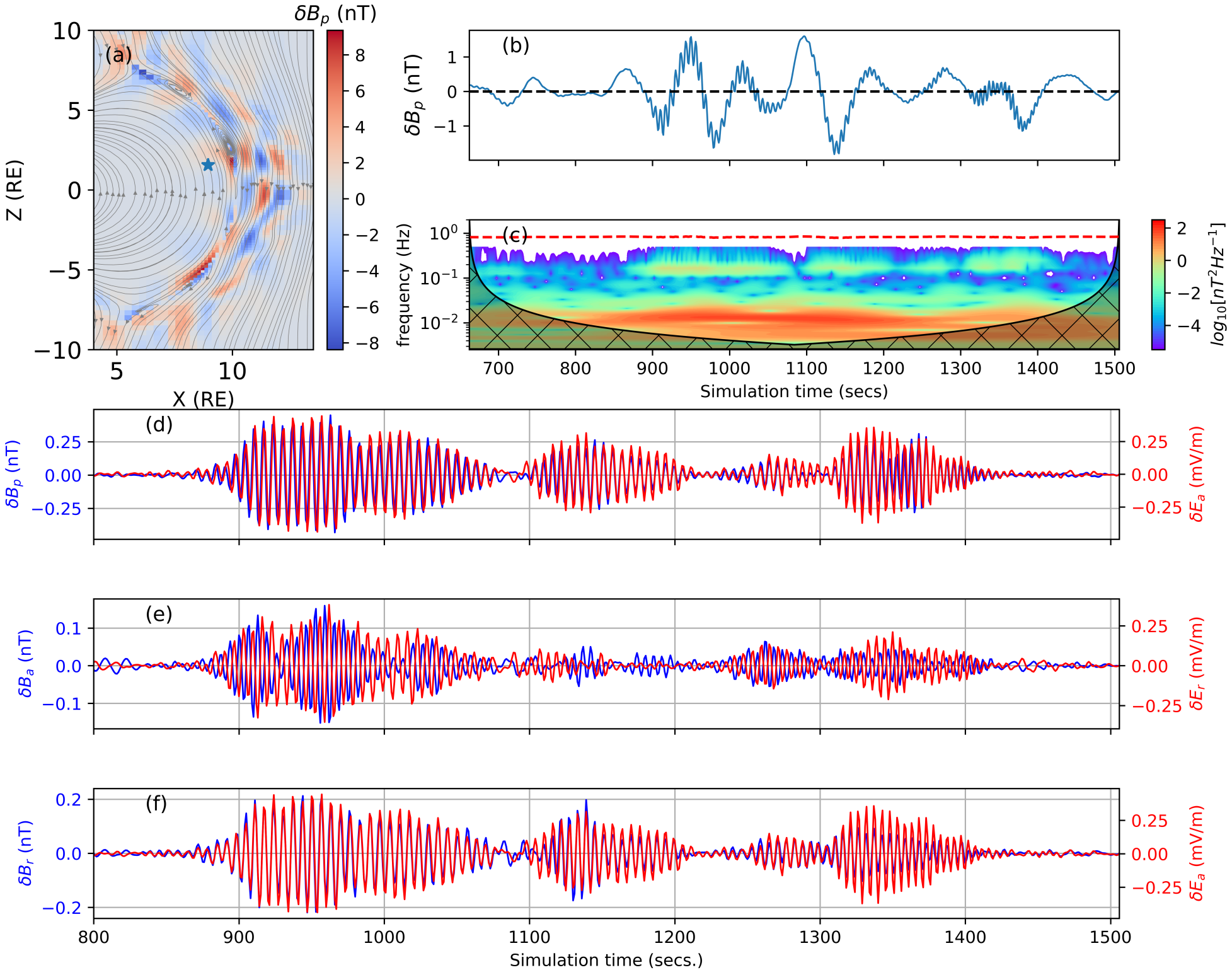
(a)
δB_p (nT)
Z (RE)
X (RE)
(b)
δB_p (nT)
(c)
frequency (Hz)
$log_{10}[nT^2Hz^{-1}]$
Simulation time (secs)
(d)
δB_p (nT)
δE_a (mV/m)
(e)
δB_a (nT)
δE_r (mV/m)
(f)
δB_r (nT)
δE_a (mV/m)
Simulation time (secs.)

Figure2.

(a) δB_p, Y = 3.5 RE
(b) δB_a, Y = 3.5 RE
(c) δB_r, Y = 3.5 RE
(d) δB_p, Y = 0 RE
(e) δB_a, Y = 0 RE
(f) δB_r, Y = 0 RE
(g) δB_p, Y = -3.5 RE
(h) δB_a, Y = -3.5 RE
(i) δB_r, Y = -3.5 RE
Z (RE)
x (RE)
10.0
7.5
5.0
2.5
0.0
−2.5
−5.0
−7.5
−10.0
6
8
10
12
10^0
10^{-1}
10^{-2}
10^{-3}
10^{-4}
0
Pc2 mean wave power (nT^2/Hz)

Figure3.

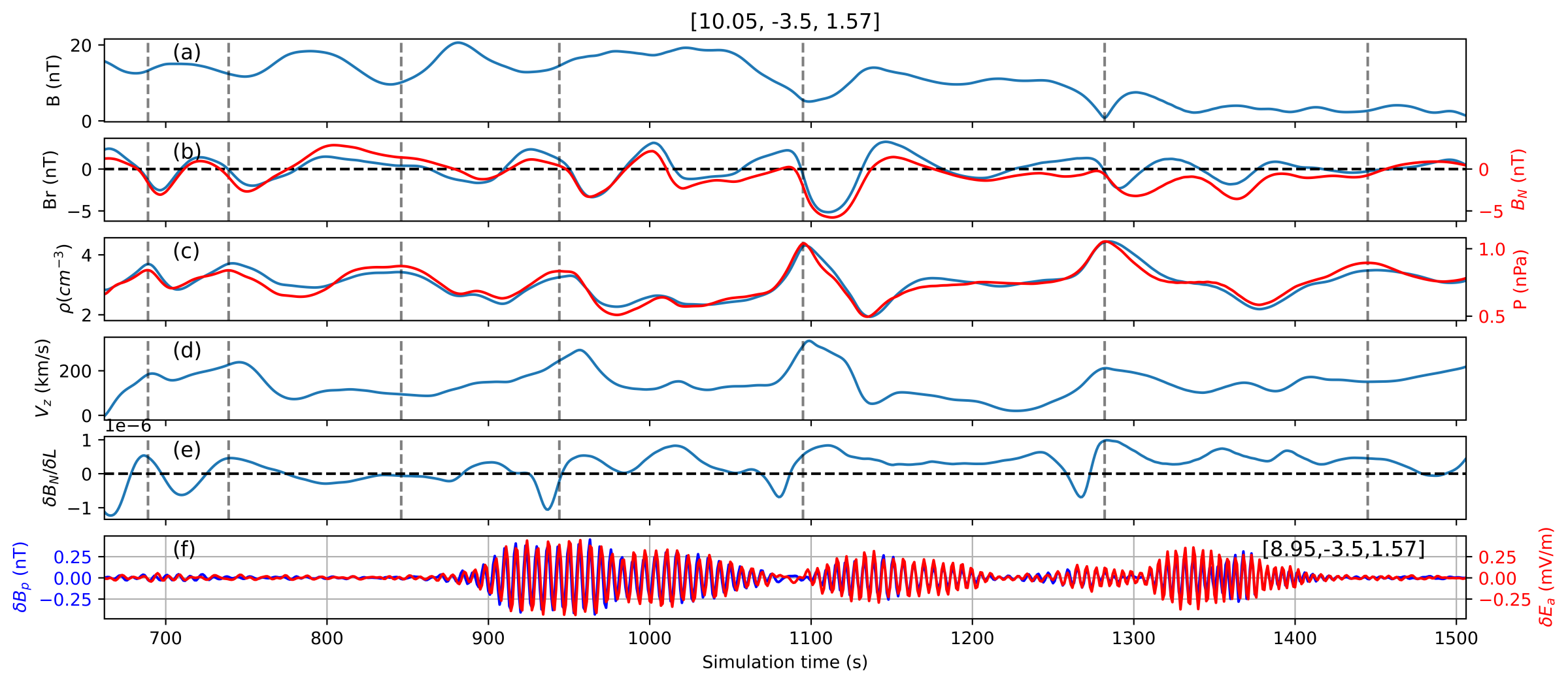
[10.05, -3.5, 1.57]
(a)
B (nT)
20
0
(b)
Br (nT)
0
−5
B_N (nT)
0
−5
(c)
$\rho(cm^{-3})$
4
2
P (nPa)
1.0
0.5
(d)
V_z (km/s)
200
0
1e−6
(e)
$\delta B_N/\delta L$
1
0
−1
(f)
[8.95,-3.5,1.57]
δB_p (nT)
0.25
0.00
−0.25
δE_a (mV/m)
0.25
0.00
−0.25
700
800
900
1000
1100
1200
1300
1400
1500
Simulation time (s)

Figure4.

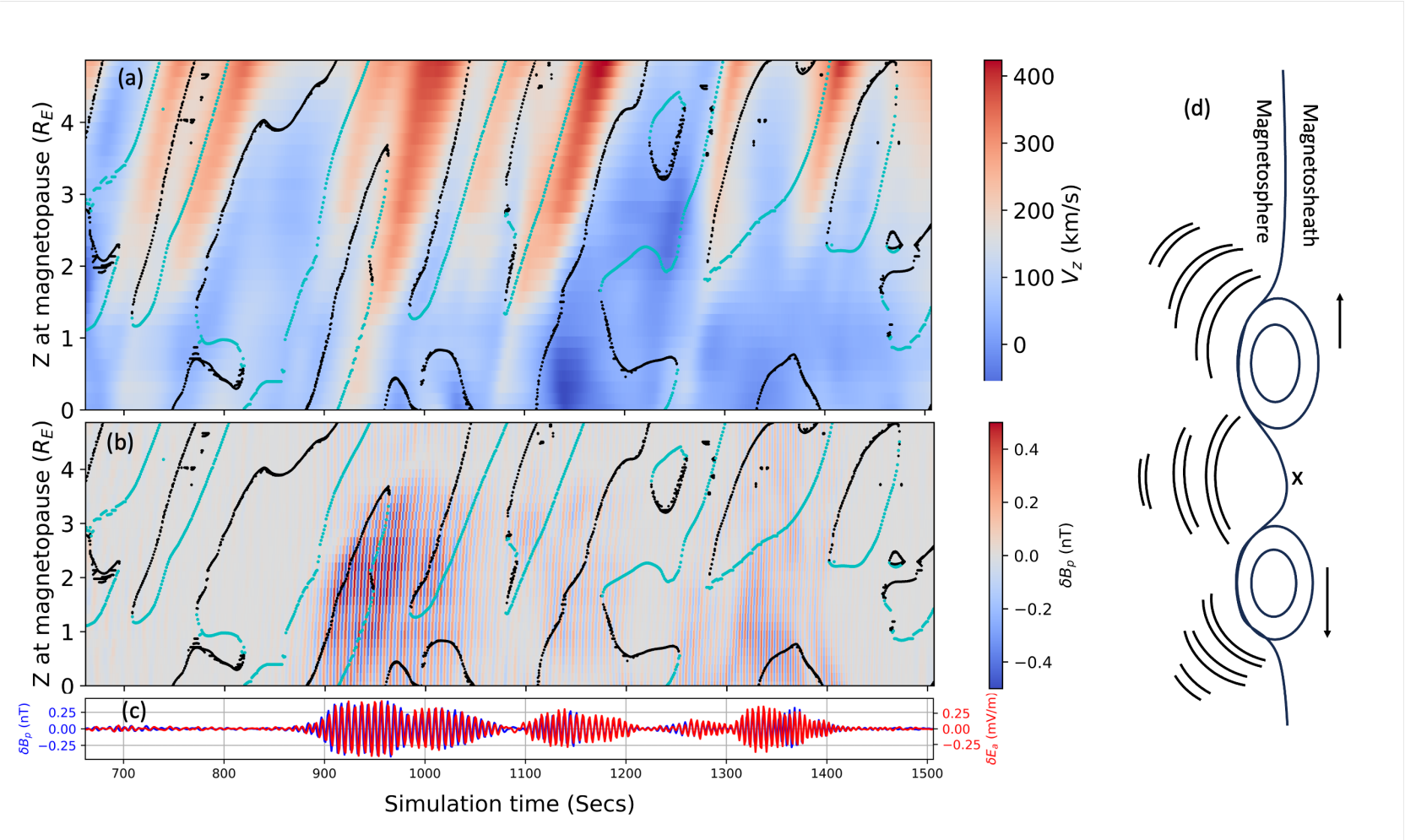
(a)
(b)
(c)
(d)
Z at magnetopause (R_E)
V_z (km/s)
δB_p (nT)
δE_a (mV/m)
Simulation time (Secs)
Magnetosheath
Magnetosphere
X